JMEPEG
https://doi.org/10.1007/s11665-022-07477-x

1059-9495/$19.00

TECHNICAL ARTICLE

Evaluation of Residual Stress Fields in Friction Stir Welded Zone Based on the Plastic Strain Increment and Mises Yield Criterion

Yiyang Li, Jiaye Zhao, Jiangfan Zhou, Yang Yang, Xianfu Huang, and Zhanwei Liu

Submitted: 11 April 2022 / Revised: 31 July 2022 / Accepted: 7 September 2022

The residual stress generated during the welding process affects the mechanical properties of the material. In this study, a measurement method of residual stress fields in the friction stir welded zone is developed based on the plastic strain increment and Mises yield criterion. First, the relationship among the residual stress, the measured local yield strength, and the plastic strain increment is derived according to the Mises yield criterion. Then, through uniaxial tensile tests, the stress–strain curve of any point in the friction stir welded zone is obtained using the digital image correlation method. Finally, the distribution of residual stress around the friction stir welded zone is characterized by the derived relationship on the basis of accurately obtaining the local yield strength. The feasibility of the method developed in this paper for measuring residual stress is verified by comparison with the results of the mechanical method combined with the charge coupled device Moiré method. Additionally, other material parameters such as modulus and yield strength can also be measured at the same time. The proposed method is applied to a mechanical properties evaluation of the friction stir welded joint of an aluminum alloy 6061T6 thin plate. The results show that the residual stress around the weld is tensile, showing a bimodal distribution, and the peak value of the residual stress is located in the thermomechanical affected zone. The strength has a double-valley distribution, and the local yield strength of the thermomechanical affected zone is the lowest. The mechanical properties of the thermomechanical affected zone are relatively poor, and it is the location that is prone to fracture.

Keywords aluminum alloy, DIC method, friction stir welding, mises yield criterion, plasticity theory, residual stress field

1. Introduction

In recent years, friction stir welding, as an important and high potential technology in the welding process, has attracted much attention in the fields of aviation, aerospace, automobiles, ships, and so on. Friction stir welding can adapt to various joint forms and different welding positions and has the advantages of small joint deformation and good mechanical properties. Friction stir welding of aluminum alloy has been widely used in the aerospace industry. The mechanical properties of aluminum alloy friction stir welded joints have always been a concern of the industry, especially the residual stress distribution, strength, and microstructure of the materials at the joints. Friction stir welded components can be divided into the weld nugget zone, thermomechanical affected zone, heat affected zone, and base material zone based on the observation and study of the microstructure of friction stir welded components. The texture of friction stir welded joints is complex, and the mechanical properties clearly change (Ref 1, 2), which poses a challenge to the original measurement method.

Friction stir welding is a solid-state process. The frictional heat between the stirring head and the workpiece causes the metal to be in a thermoplastic state, which will inevitably produce welding residual stress. When using friction stir welded joints in aircraft structures, their mechanical behavior must be fully understood, especially the variation in strength and residual stress at the joints. The influence of welding parameters (pin profile, tool shoulder diameter, welding speed, rotational speed, and so on) on the mechanical properties of joints has been studied extensively (Ref 3-5). At present, the modulus and strength in a specific part of a weld can be estimated using the digital image correction (DIC) method (Ref 6-8). Srinivasa Rao tested the tensile and bending properties of aluminum alloy AA7020-T6 friction stir welded components and observed their microstructure through optical microscopy and transmission electron microscopy (Ref 9). Lemmen and Lei accurately calculated elastoplastic parameters, including yield strength, by measuring the stress–strain curve of a local area (Ref 10, 11).

Residual stress measurement methods are mainly divided into destructive, semidestructive, and nondestructive methods

Yiyang Li and **Zhanwei Liu**, School of Aerospace Engineering, Beijing Institute of Technology, Beijing 100081, China; **Jiaye Zhao**, Institute of Flexible Electronics Technology of Tsinghua, Zhejiang 314006, China; **Jiangfan Zhou**, Beijing Institute of Structure and Environment Engineering, Beijing 100076, China; **Yang Yang**, AECC Beijing Institute of Aeronautical Materials, Beijing 100095, China; and **Xianfu Huang**, State Key Laboratory of Nonlinear Mechanics (LNM), Institute of Mechanics, Chinese Academy of Sciences, Beijing 100190, China; and School of Engineering Science, University of Chinese Academy of Sciences, Beijing 100049, China. Contact e-mails: 541161785@qq.com and liuzw@bit.edu.cn.

Published online: 10 October 2022

(Ref 12, 13). Nondestructive methods are now widely employed, and common nondestructive testing methods include x-ray diffraction, neutron diffraction, ultrasound, and magnetic measurements. Based on localized digital image correlation technology and x-ray diffraction (XRD) technology, Lemmen measured the yield strength and residual stress distribution at the joints of 3 types and multiple processes (Ref 10). Using short wavelength x-ray diffraction (SWXRD) and neutron diffraction technology, Ji measured the residual stress distribution of 7075 aluminum alloy friction stir welded components (Ref 14).

Combined with noncontact optical strain and deformation testing methods such as the Moiré method and digital image correlation method, the stress release method for estimating residual stress has the advantages of high precision and easy operation (Ref 15). The XRD method obtains the residual stress on the surface by measuring the change in the lattice spacing on the material surface, but for materials with complex compositions and complex structures (texture or grain shape), the estimation of residual stress will be more complicated. Compared with stress release methods, nondestructive testing methods such as XRD have the disadvantages of complicated operation, high test costs, and many influencing factors. For the measurement of areas where the residual stress gradient changes greatly, point-wise distribution measurement methods such as XRD or the hole-drilling technique are complicated and time-consuming.

In this study, a method was developed to simultaneously obtain the residual stress, local yield strength, and local modulus mappings near a friction stir welded joint in a single experiment. The local stress–strain curve of the friction stir welded joint of the aluminum alloy was measured by the DIC method, and the local modulus and local yield strength mappings were obtained by combining with the yield criterion. The residual stress fields around the weld can be obtained after the relationship of the residual stress, the local yield strength, and the increase in plastic strain was derived based on the Mises yield criterion and plastic theory. The feasibility and correctness of this method were proven by comparison with the test results of the residual stress released by the charge coupled device (CCD) Moiré method and stress release method. The results show that the strength near the weld has a W-like distribution, and the residual stress has an M-like distribution. The test results are consistent with the results presented and discussed in published literature (Ref 23, 32).

2. Method of Measuring the Residual Stress Field

If a component is in a state of plane stress and a point reaches yield, then, according to the Mises yield condition, the two principal stresses σ_1 and σ_2 at that point and the yield strength σ_s of the material satisfy the relationship (Ref 16):

$$\sigma_1^2 + \sigma_2^2 - \sigma_1\sigma_2 = \sigma_s^2 \quad \text{(Eq 1)}$$

If σ_1 is taken as an independent variable and σ_2 is regarded as an unknown variable, then σ_2 can be obtained by Eq 1:

$$\sigma_2 = \frac{1}{2}\left(\sigma_1 \pm \sqrt{4\sigma_s^2 - 3\sigma_1^2}\right)\left(-\frac{2}{\sqrt{3}}\sigma_s \le \sigma_1 \le \frac{2}{\sqrt{3}}\sigma_s\right) \quad \text{(Eq 2)}$$

Equation 2 takes the derivative of σ_1 as the slope K of the tangent line at any point on the in-plane yield curve ellipse:

$$K = \sigma_2' = \frac{1}{2}\left(1 \pm \frac{3\sigma_1}{\sqrt{4\sigma_s^2 - 3\sigma_1^2}}\right) \quad \text{(Eq 3)}$$

The slope α of the normal at any point on the in-plane yield curve ellipse is:

$$\alpha = -\frac{1}{K} = \frac{2\sqrt{4\sigma_s^2 - 3\sigma_1^2}}{\pm 3\sigma_1 - \sqrt{4\sigma_s^2 - 3\sigma_1^2}} \quad \text{(Eq 4)}$$

In the stress space, both the stress state and the strain state of a point can be represented by vectors. Since the principal axis of stress and principal axis of strain in elastic deformation coincide, when a small area begins to deform plastically (yield), the principal axis of stress and strain at that area also coincide. The vector of the plastic deformation increment must be perpendicular to the yield surface according to the flow law of plasticity theory (Ref 17). Therefore, the outer normal of any small area on the yield surface coincides with the vector of the plastic deformation increment. In the plane stress state, the slope α of the outer normal line represents the ratio of the plastic deformation increments in the two principal stress directions:

$$\alpha = \frac{\Delta\varepsilon_2^\rho}{\Delta\varepsilon_1^\rho} \quad \text{(Eq 5)}$$

where $\Delta\varepsilon_1^\rho$ and $\Delta\varepsilon_2^\rho$ are the plastic strain increments in the first and second principal stress directions, respectively.

$$\begin{cases} \Delta\varepsilon_1^\rho = \varepsilon_1^\rho(p_2) - \varepsilon_1^\rho(p_1) \\ \Delta\varepsilon_2^\rho = \varepsilon_2^\rho(p_2) - \varepsilon_2^\rho(p_1) \end{cases} \quad \text{(Eq 6)}$$

The strain of the specimen at each moment during the tensile process can be obtained by the DIC method. Combined with the stress–time curves generated by the tensile machine, the strain at each stress can be obtained. Taking the stress $\sigma(p_1)$ and $\sigma(p_2)$ under two external loads p_1 and p_2 after entering the plastic phase, the strain in the first principal stress direction corresponding to the stress is $\varepsilon_1^\rho(p_1)$ and $\varepsilon_1^\rho(p_2)$, and the strain in the second principal stress direction is $\varepsilon_2^\rho(p_1)$ and $\varepsilon_2^\rho(p_2)$. Then, α can be determined.

Equation 4 can be rewritten as:

$$\sigma_1 = \pm\frac{2|2+\alpha|}{\sqrt{9\alpha^2 + 3(2+\alpha)^2}}\sigma_s \quad \text{(Eq 7)}$$

Let

$$f_1(\alpha) = \frac{2|2+\alpha|}{\sqrt{9\alpha^2 + 3(2+\alpha)^2}}\left(-\frac{1}{2} \le \alpha \le 1\right) \quad \text{(Eq 8)}$$

According to Eqs 7 and 2,

$$\sigma_1 = f_1(\alpha)\sigma_s, -\frac{1}{2} \le \alpha \le 1$$

$$\begin{cases} \sigma_2 = \frac{1}{2}\left[f_1(\alpha) + \sqrt{4 - 3f_1^2(\alpha)}\right], 0 \le \alpha \le 1 \\ \sigma_2 = \frac{1}{2}\left[f_1(\alpha) - \sqrt{4 - 3f_1^2(\alpha)}\right], -\frac{1}{2} \le \alpha \le 0 \end{cases} \quad \text{(Eq 9)}$$

The main stress direction of the welding residual stress is usually perpendicular to the welding seam and parallel to the

welding seam. Therefore, the residual stress σ_{1r}, σ_{2r} of the measuring point in the two main stress directions and the main stress $\sigma_1(p), \sigma_2(p)$ under the applied external load p should meet the formula:

$$\begin{aligned} \sigma_1 &= \sigma_{1r} + \sigma_1(p) \\ \sigma_2 &= \sigma_{2r} + \sigma_2(p) \end{aligned} \quad \text{(Eq 10)}$$

when the material yields under the external load p_s,

$$\begin{aligned} \sigma_{1r} &= \sigma_1 - \sigma_1(p_s) \\ \sigma_{2r} &= \sigma_2 - \sigma_2(p_s) \end{aligned} \quad \text{(Eq 11)}$$

For isotropic materials,

$$\begin{aligned} \sigma_1(p_s) &= \frac{E}{1-v^2}[\varepsilon_1(p_s) + v\varepsilon_2(p_s)] \\ \sigma_2(p_s) &= \frac{E}{1-v^2}[\varepsilon_2(p_s) + v\varepsilon_1(p_s)] \end{aligned} \quad \text{(Eq 12)}$$

In the uniaxial tensile load condition ($0 \le \alpha \le 1$), according to Eqs 9, 11, and 12 to obtain:

$$\begin{aligned} \sigma_{1r} &= f_1(\alpha)\sigma_s - \sigma_1(p_s) \\ \sigma_{2r} &= \frac{1}{2}\left[f_1(\alpha) + \sqrt{4 - 3f_1^2(\alpha)}\right]\sigma_s \end{aligned} \quad \text{(Eq 13)}$$

If the material is known, then σ_s is certain, so as long as $f_1(\alpha)$ and $\sigma_1(p_s)$ are measurable, the residual stress can be determined.

Using the localized DIC method (Ref 11), the stress–strain curve at a certain point and the strain increments (for example, within $[p_s, 1.01p_s]$) in two directions can be obtained. By substituting Eq 5 into Eq 8, $f_1(\alpha)$ can be calculated. The stress corresponding to the 0.2% yield strain on the stress–strain curve is taken as the measured yield stress $\sigma_1(p_s)$ at this point. As shown in Fig. 1, the stress–strain curve is first drawn in the y- and x-directions (first and second principal stress directions, respectively). The slope of the elasticity phase obtained by fitting is the modulus of this point in the y-direction, and the stress corresponding to the load producing 0.2% residual deformation is taken as the measured yield stress $\sigma_1(p_s)$, Then, in the interval $[p_s, 1.01p_s]$, that is, within the same time interval, intercept the sum of the plastic deformation increments $\Delta\varepsilon_1^\rho = \Delta\rho_1$ and $\Delta\varepsilon_2^\rho = \Delta\rho_2$ in the y- and x-directions, and calculate the slope α according to Eq 5. Finally, calculate the residual stress σ_{1r}, σ_{2r} through Eq 8 representing the transformation of α and Eq 13 representing the relationship of the residual stress, the measured yield strength, and the plastic strain increment. After obtaining the data of all points in the area according to the above method, the mapping of the local modulus, local yield strength, and residual stress can be characterized at the same time.

3. Experimental

3.1 Specimen Preparation

In this paper, the size of the sample with a friction stir welding area is shown in Fig. 2. The base material is aluminum alloy 6061T6, the modulus is 60 GPa, and the yield strength is 250 MPa. The sample was cut from a friction stir welded thin plate of aluminum alloy 6061T6, and the plate thickness is 3 mm. The processing parameters are shown in Table 1.

Generally, the vicinity of friction stir welded joints can be divided into a WN (weld nugget), a TMAZ (thermomechanical affected zone), and an HAZ (heat affected zone) according to the microscopic results (Ref 18). The TMAZ is located between the HAZ and the WN and is located near the shaft shoulder, and its microstructure has obvious rotating textures. AS represents the advancing side when the friction stir welding shaft shoulder rotates, and RS represents the retreating side. The mechanical properties of the WN, TMAZ, and HAZ are different. The zone division and direction of friction stir welding are shown in Fig. 3.

3.2 Uniaxial Tension Testing

The uniaxial tensile test is used to obtain the mechanical properties of the aluminum alloy friction stir welded joints. The stretching direction is the same as the longitudinal direction in Fig. 3, and there are speckles on the surface of the specimen. A Daheng Mercury Series CMOS camera was used to take pictures during the stretching experiment, and the 2D-DIC method was used to obtain the deformation and strain information at the joints. The optical axis of the camera was parallel to the normal direction in Fig. 3 and 4. In this experiment, the loading speed was 1 mm/min, the image acquisition rate was 1 fps, and the image resolution was 2448 × 1942 pixels.

4. Results and Analysis

4.1 Tensile Test Results

First, the strain field at each moment was calculated using the speckle images of the specimen surface during the stretching process taken by the camera. The strain field near the 6061T6 aluminum alloy friction stir welded joint during the stretching process under 7 and 12 kN tensile loads is shown in Fig. 5. The strain field was calculated by Ncorr (open-source 2D digital image correlation MATLAB software) (Ref 19).

The stress–strain curve for each small area in the selected region can be obtained by combining the time and load data generated by the testing machine and the strain field at each moment, provided that the specimen size is determined. The photograph in Fig. 6 shows a part of a tensile specimen with speckle near the friction stir welded joint of aluminum alloy 6061T6. According to the size of the weld area and the test requirements, the size of the area is reasonably selected as m × n pixels. The typical stress–strain curves (in the same direction) of five colored areas located in the regions of the HAZ (left), TMAZ (left), WN, TMAZ (right), and HAZ (right) are given. Modulus, yield strength, and residual stress can be calculated according to the methods described in Sect. 2. The slope of the elasticity phase obtained by fitting is the modulus. Due to the relatively large error in the DIC calculation of small deformations, the data with strains less than 0.05% were not used in the calculation of the modulus. For each stress–strain curve, the corresponding 0.2% yield strength is indicated (red sign in Fig. 6).

To show the law that the yield strength changes with position, the local yield strength of each subarea within the red area is calculated, and the x-axis coordinates represent the location of the subarea. The position of each point in the curve corresponds to the position of the subarea in the photo.

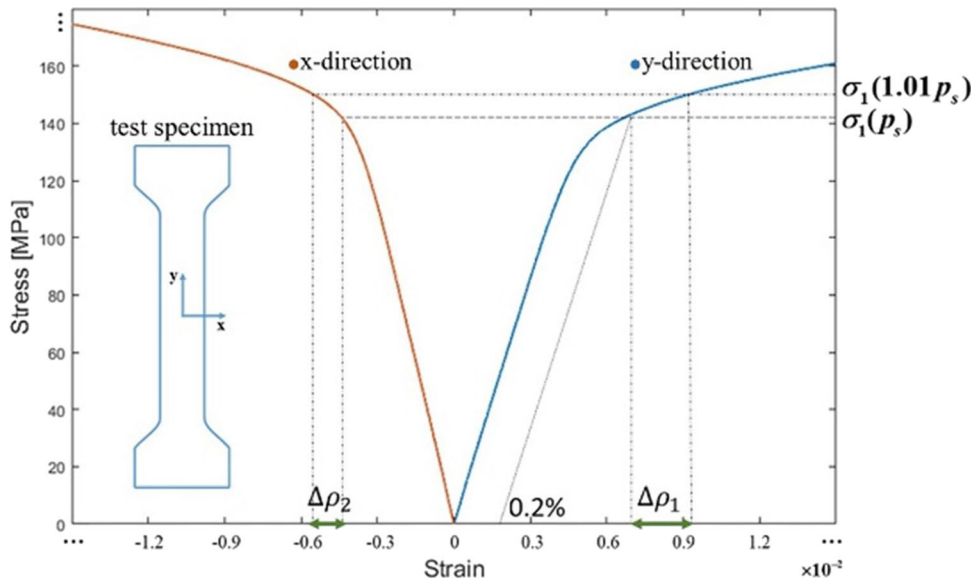

Fig. 1 Theoretical stress–strain curve

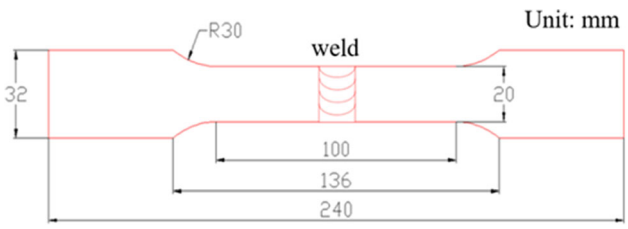

Fig. 2 Friction stir welding specimen

Table 1 Friction stir welding parameters

Welding speed	Rotational speed	Shaft shoulder	Stirring pin	Plunge depth	Tilt angle
300 mm/min	1200 rpm	10 mm	2.8 mm	2.8 mm	2.5°

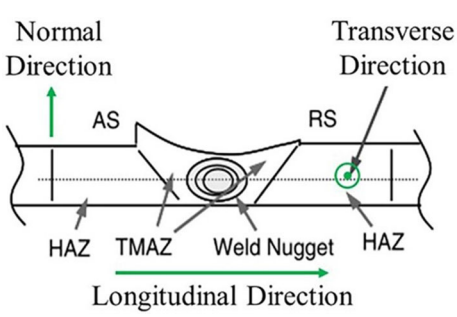

Fig. 3 Friction stir welded joint

Figures 6 and 7 show that the yield strength of the WN and TMAZ is lower than that of the HAZ. The local yield strength shows an approximately W-shaped distribution trend, which can also be seen by the color depth of the residual stress distribution graph in Fig. 8. The yield strength is not completely symmetrical due to the asymmetry of the welding process.

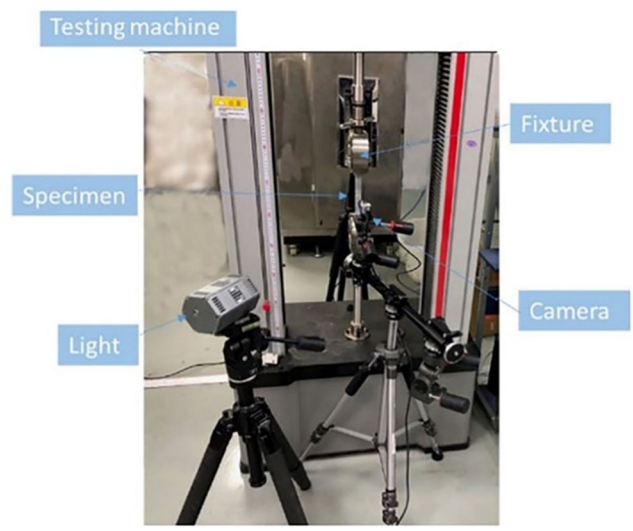

Fig. 4 Experimental device

5. Residual Stress Test Results and Fractography Analysis

Using the method proposed in Sect. 2, residual stress is obtained from the relationship of the residual stress, the local yield strength, and the plastic strain increment according to the Mises yield criterion. Notably, the local yield strength is affected by the microstructural changes and residual stress generation caused by the welding process (Ref 20, 21). The mapping of the local modulus, local yield strength, LD (longitudinal direction) residual stress, and TD (transverse direction) residual stress near the 6061T6 aluminum alloy friction stir welded joint is shown in Fig. 8. To reduce the error, the results close to the edge were not measured due to residual stress relaxation when cutting during fabrication of the specimens and the limitations of the DIC method.

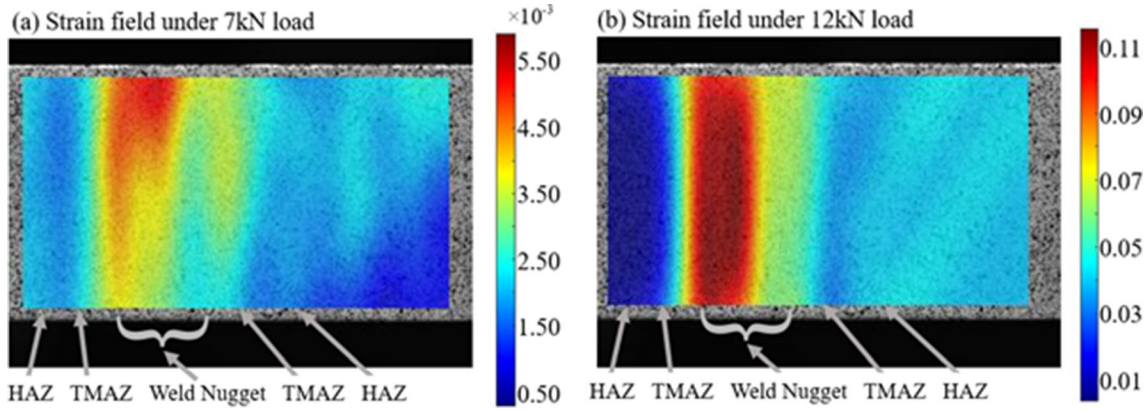

Fig. 5 Strain field during stretching (a) under a 7 kN tensile load and (b) under a 12 kN tensile load

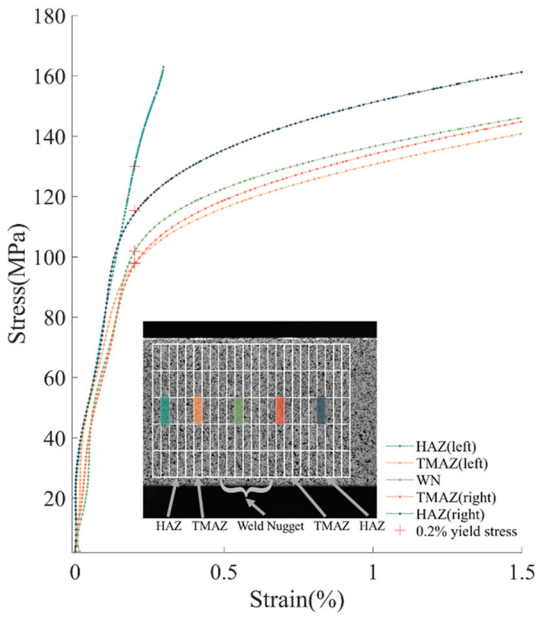

Fig. 6 The typical stress–strain curve of different regions

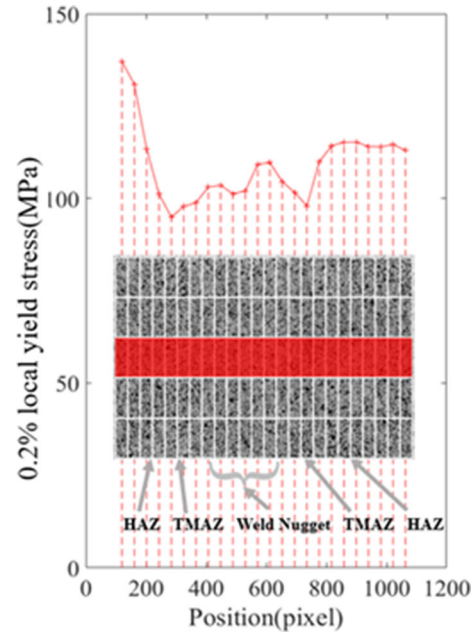

Fig. 7 0.2% local yield strength curve

The modulus of the TMAZ is significantly lower than that of the WN and HAZ, and the HAZ modulus is the highest, which is consistent with the microhardness test results (Ref 22).

The local yield strength of the TMAZ is significantly lower than that of the WN and HAZ. The lowest yield strength is 91.7 MPa in the TMAZ. The HAZ has the highest yield strength. The distribution of the local yield strength and modulus in this paper is consistent with the distribution of microhardness in the literature (Ref 22). It is clear that there is a one-to-one relationship between modulus and microhardness; some studies have shown that there is a functional relationship between yield strength and microhardness (Ref 23).

According to the related research test results, the residual stress should be less than the yield strength of the base material (Ref 24). The ratio between the maximum tensile residual stress and the base material yield strength is approximately 60% for welded joints under normal friction stir welding (Ref 25). The measured maximum residual stress is 64% of the base material yield strength, which is consistent with the relevant research.

In the LD, the residual stress of the TMAZ is significantly higher than that of the WN and HAZ, and the residual stress of the HAZ is the lowest, showing an M-shaped distribution. In the current literature, most of the residual stress measurement results in the LD of the friction stir welded joint using neutron diffraction, SWXRD, drilling, and other methods have an M-shaped distribution, and the test results in this paper are consistent with these existing studies. The LD residual stress of the left TMAZ and the right TMAZ are not completely symmetrically distributed, the AS residual stress is larger, and the larger residual stress value area is wider. This is caused by the difference in heat input between the AS and the RS during the welding process, and the AS heat input is higher, which is related to their peak temperature (Ref 26, 27). The residual stress in the TD has the same law as that in the LD.

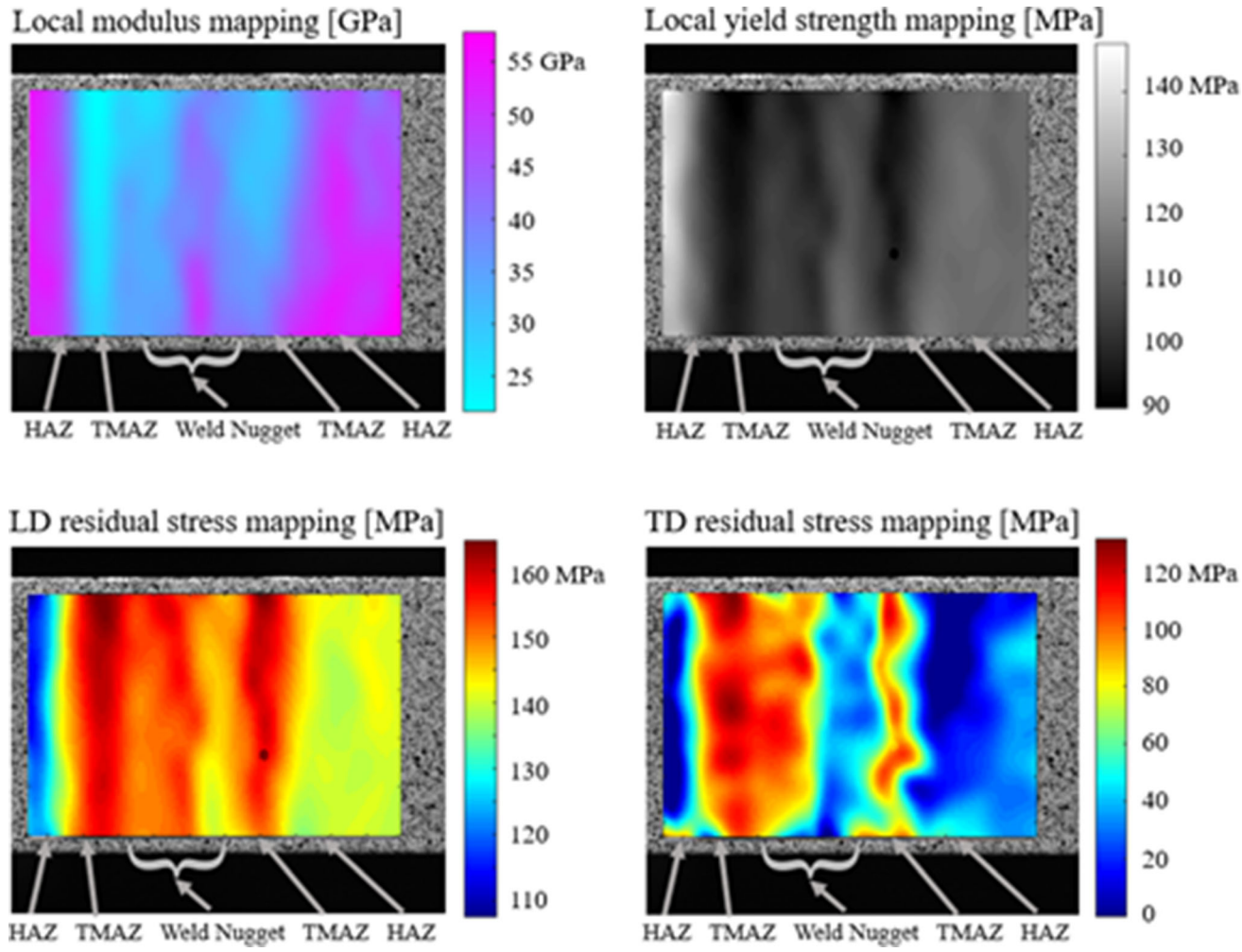

Fig. 8 Local modulus, local yield strength, LD residual stress, and TD residual stress mapping measurement results

In summary, the mechanical properties of the TMAZ at the joint are the worst. The residual stresses of the TMAZ in the LD and TD are both large, with peak values exceeding 160 MPa, and the local yield strength and modulus are the lowest. The TMAZ is the place where fractures can easily occur. The fracture of the joint in the TMAZ is shown in Fig. 9, and the fracture is sheared at 45°.

The fractographs are shown in Fig. 10. From Fig. 10(a), the fracture surface is full of dimples of different sizes, with small sizes and deep depths, which indicates that the fracture is ductile. From Fig. 10(b), the fracture mode is mainly trans-granular dimple rupture. According to the analysis of Fig. 10, compared with the grain size of the base material (Ref 28), the grain size of TMZA is smaller and mostly less than 50 μm. The TMAZ and WN are highly deformed by the material rotational flow (Ref 29). The changes in grain size will definitely cause changes in mechanical properties to some extent.

5.1 Verification of the Residual Stress Measurement Results

The CCD Moiré method and mechanical method are used to measure the residual stress of the batch of friction stir welded joints with the same welding process. The specific steps are as follows:

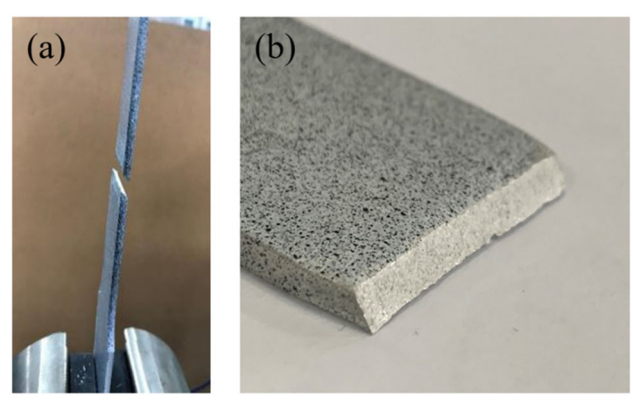

Fig. 9 Fracture macroscopic morphology of the material after tensile testing: (a) fracture specimen on the experimental machine and (b) fracture enlarged view

1. Produce 1200 lines/mm grating on the surface of the test piece;
2. Perform wire cutting at the position shown in Fig. 11(a);
3. Observe the marked points in the picture under an optical microscope, and collect the Moiré picture (Fig. 11b);

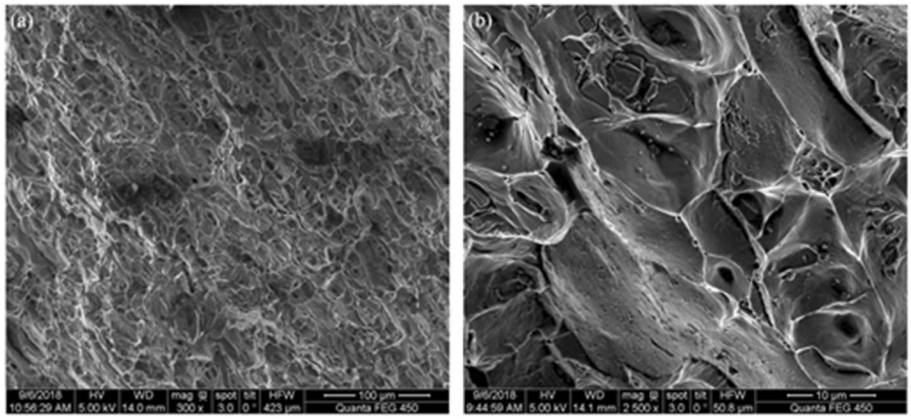

Fig. 10 Fractographs of material after tensile test: (a) mag 300 × and (b) mag 2500 ×

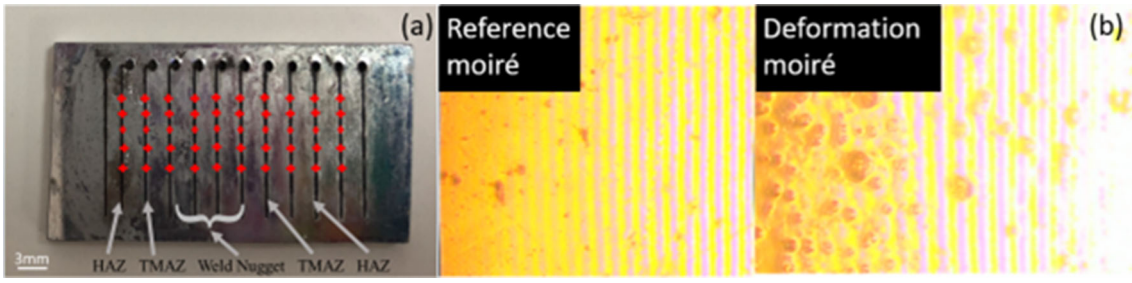

Fig. 11 Residual stress verification test: (a) specimen and (b) Moiré picture

4. Calculate the residual stress (LT) based on the collected Moiré pictures. The specific residual stress measurement method is based on paper (Ref 30).

The measurement results of the mechanical method residual stress at each point in the LD are averaged to fit the LD residual stress curve, which is compared and analyzed with the measurement results of averaging the residual stress field in the LD along the TD in this article. As shown in Fig. 12, the residual stress obtained by the mechanical method and the residual stress obtained by the method in this paper are both tensile stresses, showing an M-shaped distribution. Combined with the yield strength test results in Fig. 7, it can be found that the sum of the residual stress and yield strength at the same position of the aluminum alloy friction stir welding is about a constant value (Ref 10). The average error between the results of the mechanical method and the method in this paper is 19.7 MPa, and the relative error is approximately 8%, which is within an acceptable range to some extent. Compared with the cutting release method, the measured value of this method is larger. The possible reason is due to the assumption of the two-dimensional residual stress field. Previous studies have shown that there are also residual stresses in the ND (normal direction) of friction stir welded joints (Ref 31). In the measurement of the residual stress at the friction stir welded joint, when making 2D and 3D stress state assumptions, there is a gap between the test results. In the real case, the 3D assumption should be used to consider the residual stress release in the ND (specimen thickness direction) of the specimen. The existing studies also

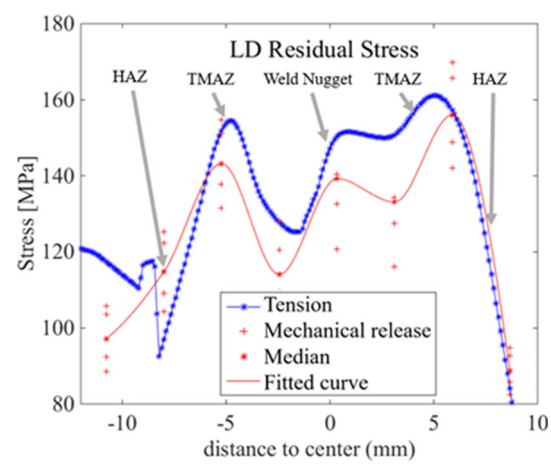

Fig. 12 Comparison of the residual stress test results

prove that the residual stress release in the ND direction has an impact on the residual stress measurement (Ref 32, 33). The specimen used in this paper was cut from a friction stir welded thin plate, which has a small deformation in the ND, so the 2D assumption is used, ignoring the residual stress release in the ND. However, the trend of the test results is consistent. The cutting process during fabrication of the specimens and the error when calculating the strain using the DIC method are also the reasons for measurement errors.

6. Conclusion

In this study, a method to characterize the residual stress mapping, the local yield strength mapping, and the local modulus mapping near the friction stir weld was developed based on the plastic strain increment and Mises yield criterion. The relationship among the local yield strength, plastic strain increment, and residual stress was derived according to the Mises yield criterion. The full-field residual stress distribution was obtained using uniaxial tensile tests and the DIC-based full-field strain measurement method. From the obtained results, the residual stress in friction stir welding of LD and TD presents an M-shaped distribution. The residual stress in the TMAZ is the largest. The residual stress of the WN is higher than that of the HAZ and lower than that of the TMAZ. This is consistent with the conclusions in the current literature (Ref 34). The mechanical properties of the TMAZ of friction stir welded joints are the worst, which is the place where tensile failure is likely to occur.

The method developed in this paper has the following advantages:

1) This method is a full-field in-plane residual stress measurement method. Compared with point-wise distribution residual stress measurement methods such as XRD or drilling methods, the residual stress measurement method developed in this paper can obtain the residual stress distribution of the entire field, and it is especially suitable for measurements in different zones of friction stir welding where the residual stress gradient changes greatly.
2) The residual stress measurement method developed in this paper has the advantages of economy, efficiency, and convenience. In addition, this method can be used to obtain the mapping of the local modulus, local yield strength, and residual stress at the same time in a uniaxial tensile test;
3) Although this paper analyzes the fracture of the test piece, this method does not need to break the test piece to obtain residual stress and can be carried out during the cold work hardening process.

Acknowledgments

This work was financially supported by the National Natural Science Foundation of China [Grant No. 11972084], National Science and Technology Major Project (2017-VI-0003-0073) and Beijing National Science Foundation (1192014).

References

1. W.F. Xu, Y.X. Luo, and M.W. Fu, Microstructure evolution in the conventional single side and bobbin tool friction stir welding of thick rolled 7085–T7452 aluminum alloy, *Mater. Charact.*, 2018, **138**, p 48–55. https://doi.org/10.1016/j.matchar.2018.01.051
2. D. Li, X. Yang, L. Cui, F. He, and H. Shen, Effect of Welding Parameters on Microstructure and Mechanical Properties of AA6061-T6 Butt Welded Joints by Stationary shoulder Friction Stir Welding, *Mater. Des.*, 2014, **64**, p 251–260. https://doi.org/10.1016/j.matdes.2014.07.046
3. M. Peel, A. Steuwer, M. Preuss, and P.J. Withers, Microstructure, mechanical properties and residual stresses as a function of welding speed in aluminium AA5083 friction stir welds, *Acta Mater.*, 2003, **51**(16), p 4791–4801. https://doi.org/10.1016/S1359-6454(03)00319-7
4. V. Moosabeiki, G. Azimi, and M. Ghayoor, Influences of Tool Pin Profile and Tool Shoulder Curvature on the Formation of Friction Stir Welding Zone in AA6061 Aluminium Alloy, *Adv. Mater. Res.*, 2012 https://doi.org/10.4028/www.scientific.net/AMR.445.789
5. Moshwan R, Yusof F, Hassan MA, and Rahmat SM. (2015). Effect of Tool Rotational Speed on Force Generation, Microstructure and Mechanical Properties of Friction Stir Welded Al-Mg-Cr-Mn (AA 5052O) Alloy. Mater Des (1980–2015). 66: 118–128
6. X. Wu, J. Shuai, K. Xu, and Z. Lv, Local Constitutive Behavior of Undermatched Welded Joints in Pipeline Steel Using Digital Image Correlation Technology, *J. Press. Vessel Technol.*, 2020, **142**, p 5. https://doi.org/10.1115/1.4047271
7. B. Chen and B. Pan, Measuring True Stress–Strain Curves of Cylindrical bar Samples with Mirror-Assisted Multi-View Digital Image Correlation, *Strain*, 2022 https://doi.org/10.1111/str.12403
8. Ł Skarżyński and J. Tejchman, Experimental investigations of fracture process using DIC in plain and reinforced concrete beams under bending, *Strain*, 2013, **49**(6), p 521–543. https://doi.org/10.1111/str.12064
9. G. Srinivasa Rao, V.V. Subba Rao, and S.R.K. Rao, Microstructure and Mechanical Properties of Welded Joints of Aluminum Alloy AA7020-T6 Obtained by Friction Stir Welding, *Metal Sci. Heat Treat.*, 2017 https://doi.org/10.1007/s11041-017-0117-x
10. H.J.K. Lemmen, R.C. Alderliesten, R.R.G.M. Pieters, R. Benedictus, and J.A. Pineault, Yield Strength and Residual Stress Measurements on Friction-Stir-Welded Aluminum Alloys, *J. Aircr.*, 2010, **47**(5), p 1570–1583. https://doi.org/10.2514/1.C000212
11. R. Bai, Y. Wei, Z. Lei, H. Jiang, W. Tao, C. Yan, and X. Li, Local Zone-Wise Elastic-plastic Constitutive Parameters of Laser-Welded Aluminium Alloy 6061 using Digital Image Correlation, *Opt. Lasers Eng.*, 2018, **101**, p 28–34. https://doi.org/10.1016/j.optlaseng.2017.09.023
12. N.S. Rossini, M. Dassisti, K.Y. Benyounis, and A.G. Olabi, Methods of Measuring Residual Stresses in Components, *Mater. Des.*, 2012, **35**, p 572–588. https://doi.org/10.1016/j.matdes.2011.08.022
13. X. Huang, Z. Liu, and H. Xie, Recent Progress in Residual Stress Measurement Techniques, *Acta Mech. Solida Sin.*, 2013, **26**(6), p 570–583. https://doi.org/10.1016/S0894-9166(14)60002-1
14. P. Ji, Z. Yang, J. Zhang, L. Zheng, V. Ji, and V. Klosek, Residual Stress Distribution and Microstructure in the Friction Stir Weld of 7075 Aluminum Alloy, *J. Mater. Sci.*, 2015, **50**(22), p 7262–7270. https://doi.org/10.1007/s10853-015-9280-x
15. J. Lu, *Handbook of Measurement of Residual stresses*, Bethel, SEM, 1996, p 319–22
16. R. Von Mises, Mechanics of the Ductile form Changes of Crystals, *Z. Fur Angew. Math. Und Mech.*, 1928, **8**, p 161–185. https://doi.org/10.1002/zamm.19280080302
17. H.H.Y.N.W. Gao, Y. Huang, W.D. Nix, and J. Hutchinson, Mechanism-based Strain Gradient Plasticity—I. Theory, *J. Mech. Phys. Solids*, 1999, **47**(6), p 1239–1263. https://doi.org/10.1016/S0022-5096(98)00103-3
18. M.W. Mahoney, C.G. Rhodes, J.G. Flintoff, W.H. Bingel, and R.A. Spurling, Properties of Friction-Stir-Welded 7075 T651 Aluminum, *Metall. Mater. Trans. A.*, 1998, **29**(7), p 1955–1964. https://doi.org/10.1007/s11661-998-0021-5
19. J. Blaber, B. Adair, and A. Antoniou, Ncorr: Open-Source 2D Digital Image Correlation Matlab Software, *Experim. Mech.*, 2015 https://doi.org/10.1007/s11340-015-0009-1
20. R.K.R. Singh et al., The Microstructure and Mechanical Properties of Friction stir Welded Al-Zn-Mg Alloy in as Welded and Heat Treated Conditions, *Mater. Des.*, 2011, **32**(2), p 682–687. https://doi.org/10.1016/j.matdes.2010.08.001
21. N.-V. Nguyen, T.-H. Pham, and S.-E. Kim, Microstructure and Strain Rate Sensitivity Behavior of SM490 Structural Steel Weld Zone Investigated Using Indentation, *Constr. Build. Mater.*, 2019, **206**, p 410–418. https://doi.org/10.1016/j.conbuildmat.2019.02.013
22. Y.X. Huang, L. Wan, Z.L. Lv, S.X. Lv, L. Zhou, and J. Feng, Microstructure and Microhardness of Aluminium Alloy Friction stir Welds with Heat Treatment, *Sci. Technol. Weld. Joining*, 2016, **21**(8), p 638–644. https://doi.org/10.1080/13621718.2016.1152748
23. I. Hejazi and S.E. Mirsalehi, Mechanical and Metallurgical Characterization of AA6061 Friction Stir Welded Joints using Microhardness

Map, *Trans. Nonf. Metals Soc. China*, 2016, **26**(9), p 2313–2319. https://doi.org/10.1016/S1003-6326(16)64351-0
24. I. Hejazi and S.E. Mirsalehi, Mechanical and Metallurgical Characterization of AA6061 Friction Stir Welded Joints using Microhardness Map, *Trans. Nonf. Metals Soc. China*, 2016, **26**(9), p 2313–2319. https://doi.org/10.1016/S1003-6326(16)64351-0
25. X. Liu, P. Xie, R. Wimpory, W. Li, R. Lai, M. Li, D. Chen, Y. Liu, and H. Zhao, Residual Stress, Microstructure and Mechanical Properties in Thick 6005A–T6 Aluminium Alloy Friction Stir Welds, *Metals*, 2019, **9**(7), p 803. https://doi.org/10.3390/met9070803
26. I. Alinaghian, S. Amini, and M. Honarpisheh, Residual Stress, Tensile Strength, and Macrostructure Investigations on Ultrasonic Assisted Friction Stir Welding of AA 6061–T6, *J. Strain Anal. Eng. Des.*, 2018, **53**(7), p 494–503. https://doi.org/10.1177/0309324718789768
27. Sheng Lu et al., Microstructures and mechanical properties of Mg alloy FSW joint characterized with asymmetric gradient in three dimension, *Materials Science Forum*. Trans Tech Publications Ltd, Stafa-Zurich, 2013, p 104–121
28. S.L. Li, Z.Q. Huang, F.L. Jiang, W.P. Chen, Z.M. Liu, and W.J. Qi, Effect of Solution Temperature on Microstructure and Property of a 6061 Aluminum Alloy, *Transact. Mater. Heat Treat.*, 2013, **34**(5), p 131–136. https://doi.org/10.13289/j.issn.10096264.2013.05.026
29. A. Simar, Y. Bréchet, B. De Meester, A. Denquin, C. Gallais, and T. Pardoen, Integrated Modeling of Friction Stir Welding of 6xxx Series Al Alloys: Process, Microstructure and Properties, *Prog. Mater. Sci.*, 2012, **57**(1), p 95–183. https://doi.org/10.1016/j.pmatsci.2011.05.003
30. H. Zhang, C. Wu, Z. Liu, and H. Xie, A Curved Surface Micro-Moire Method and its Application in Evaluating Curved Surface Residual Stress, *Measure. Sci. Technol.*, 2014, **25**(9), p 095002. https://doi.org/10.1088/0957-0233/25/9/095002
31. Y. Guo, X. Zhang, X. Qian, and J. Li, Study on Residual Stress Distribution of 2024–T3 and 7075–T6 Aluminum Dissimilar Friction Stir Welded Joints, *Eng. Fail. Anal.*, 2020, **118**, p 104911. https://doi.org/10.1016/j.engfailanal.2020.104911
32. W. Woo et al., Neutron Diffraction Measurements of Residual Stresses in Friction Stir Welding: A Review, *Sci. Technol. Weld. Join.*, 2011, **16**(1), p 23–32. https://doi.org/10.1179/136217110X12731414739916
33. Michael B. Prime et al., Residual Stress Measurements in a Thick, Dissimilar Aluminum Alloy Friction Stir Weld, *Acta Mater.*, 2006, **54**(15), p 4013–4021. https://doi.org/10.1016/j.actamat.2006.04.034
34. W. Woo and H. Choo, Softening Behaviour of Friction Stir Welded Al 6061–T6 and Mg AZ31B Alloys, *Sci. Technol. Weld. Join.*, 2011, **16**(3), p 267–272. https://doi.org/10.1179/1362171811Y.0000000016